A Letters Journal Exploring the Frontiers of Physics

July 2016

EPL, **115** (2016) 14005
doi: 10.1209/0295-5075/115/14005

www.epljournal.org

$\mathcal{PT}$-symmetry in Rydberg atoms

Ziauddin[1,2,3(a)], You-Lin Chuang[1,3] and Ray-Kuang Lee[1,3(b)]

[1] *Institute of Photonics and Technologies, National Tsing-Hua University - Hsinchu 300, Taiwan*
[2] *Quantum Optics Lab. Department of Physics, COMSATS institute of information technology - Islamabad, Pakistan*
[3] *Physics Division, National Centre for Theoretical Science - Hsinchu 300, Taiwan*

received 28 January 2016; accepted in final form 14 July 2016
published online 8 August 2016

PACS 42.50.Gy – Effects of atomic coherence on propagation, absorption, and amplification of light; electromagnetically induced transparency and absorption
PACS 11.30.Er – Charge conjugation, parity, time reversal, and other discrete symmetries
PACS 78.20.Ci – Optical constants (including refractive index, complex dielectric constant, absorption, reflection and transmission coefficients, emissivity)

Abstract – We propose a scheme to realize parity-time ($\mathcal{PT}$)-symmetry in an ensemble of strongly interacting Rydberg atoms, which act as superatoms due to the dipole blockade mechanism. We show that Rydberg-dressed ^{87}Rb atoms in a four-level inverted Y-type configuration is highly efficient to generate the refractive index for a probe field, with a symmetric (antisymmetric) profile spatially in the corresponding real (imaginary) part. Comparing with earlier investigations, the present scheme provides a versatile platform to control the system from $\mathcal{PT}$-symmetry to non-$\mathcal{PT}$-symmetry via different external parameters, *i.e.*, coupling field detuning, probe field intensity and control field intensity.

Introduction. – Every physical observable in quantum mechanics requires a real spectrum with a Hermitian Hamiltonian, nevertheless, Bender and co-workers claimed that non-Hermitian Hamiltonians can have real spectra under the parity ($\mathcal{P}$) and time ($\mathcal{T}$) symmetries of physical systems [1]. Even though, it was pointed out that the no-signaling principle will be violated when applying the local $\mathcal{PT}$-symmetric operation on one of the entangled particles [2], $\mathcal{PT}$-symmetry could still be used as an interesting model for open systems in classical limit. Based on the equivalence between the Schrödinger equation and the optical wave equation, $\mathcal{PT}$-symmetry in classical optical systems demands that the real and imaginary parts of a complex potential must be even and odd functions, *i.e.*, $V(x) = V^*(-x)$. The concept of $\mathcal{PT}$-symmetry was then demonstrated in waveguides with gain and loss [3–6]. The realization of $\mathcal{PT}$-symmetry has prompted many designs of $\mathcal{PT}$-synthetic materials exhibiting various interesting characteristics. These include for example, unidirectional reflectionless wave propagation [7–9], coherent perfect absorber [10,11], giant wave amplification [12], and giant Goos-Hänchen shift [13]. Experimental realization of $\mathcal{PT}$-symmetry has also been reported in plasmonics [14], synthetic lattices [15], and LRC circuits [16]. In addition to solid-state media and optical devices, $\mathcal{PT}$-symmetry was studied in atomic media [17–19]. In ref. [17], Hang and co-workers considered two species of gain and loss atomic systems in the Λ-type configuration. In atomic systems, one may have many attractive characteristics, such as that the optical structures can be easily tuned and controlled in atomic medium through different external parameters, *i.e.*, strength of Rabi frequencies and detunings. In another work of Sheng and co-workers [19], a single species of four-level N-type atomic medium has been considered for the realization of $\mathcal{PT}$-symmetry. The control over non-$\mathcal{PT}$- and $\mathcal{PT}$-symmetries was achieved by adjusting the coupling frequency detunings and introduced gain and loss in a system simultaneously. Recently, nonlinear wave dynamics has been studied in $\mathcal{PT}$-symmetric systems and reported the relation between non-linearity and $\mathcal{PT}$-symmetry that generated a new phenomena [20].

Further, Rydberg states with a high principal quantum number was demonstrated to address electromagnetically induced transparency (EIT) in atomic ensembles [21]. There exists a strong interaction among the Rydberg atoms, which is known as a dipole blockade [22]. In Rydberg-dressed atoms, one Rydberg excitation can block the Rydberg excitation of all atoms in its surrounding volume. Rydberg-dressed EIT systems in the three-level

(a) E-mail: ziauddin@comsats.edu.pk (corresponding author)
(b) E-mail: rklee@ee.nthu.edu.tw

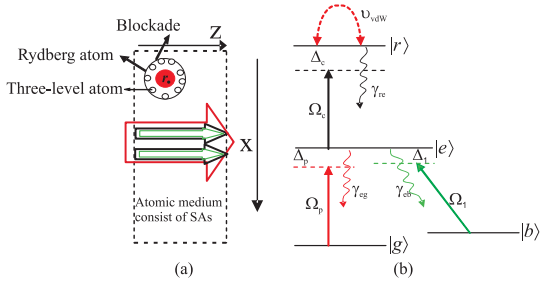

Fig. 1: (Color online) (a) The schematics of the light incident on a medium. x and z are the transverse and longitudinal direction of propagation, respectively. (b) The energy-level configuration of the inverted Y-type system.

cascade configuration was proposed, with the transparency window controlled by the strength of probe field [23]. In this work, we extend the concept of the three-level cascade system to a four-level inverted Y-type configuration, and exploit the realization of $\mathcal{PT}$-symmetry in Rydberg atomic medium. We take the van der Waals (vdW) interaction between atoms into considerations, and control the $\mathcal{PT}$- and non-$\mathcal{PT}$-symmetries using external parameters. With coupling field detunings to balance the gain and loss in a system simultaneously, our proposed Rydberg atoms provides a versatile platform to investigate $\mathcal{PT}$-symmetry with the dipole blockade.

Model. – We consider an ensemble of ^{87}Rb atoms in inverted Y-type atomic configuration interacting with three optical fields. The probe (red), coupling (black) and control (green) fields interacting with atomic medium as depicted in fig. 1(b). Each atom has energy-levels $|g\rangle$, $|e\rangle$, $|b\rangle$ and $|r\rangle$. A probe field of frequency ω_p drives the transition between $|g\rangle$ and $|e\rangle$ with Rabi frequency Ω_p, whereas the control field with Rabi frequency Ω_c drives the transition between $|r\rangle$ and $|e\rangle$ and a third field is applied between $|e\rangle$ and $|b\rangle$ with Rabi frequency Ω_1. The coupling field excites the atoms to the Rydberg state $|r\rangle$ and the atoms interact with each other via a vdW potential $\Delta(\mathbf{r}_i - \mathbf{r}_j) = C_6/|\mathbf{r}_i - \mathbf{r}_j|^6$ [23], where $\mathbf{r}_i$ and $\mathbf{r}_j$ are the positions of atoms i and j, respectively. The total Hamiltonian can then be written as

$$H = H_a + H_{af} + H_{\rm vdW}, \tag{1}$$

where

$$\begin{aligned} H_a &= -\hbar \sum_j^N [\Delta_p \sigma_{ee}^j + \Delta_2 \sigma_{rr}^j + (\Delta_p - \Delta_1)\sigma_{bb}^j], \\ H_{af} &= -\hbar \sum_j^N [\Omega_p \sigma_{eg}^j + \Omega_c \sigma_{re}^j + \Omega_1 \sigma_{eb}^j + \text{H.c.}], \\ H_{\rm vdW} &= \hbar \sum_{i<j}^N \sigma_{rr}^i \Delta(\mathbf{r}_i - \mathbf{r}_j)\sigma_{rr}^j, \end{aligned} \tag{2}$$

whereas $\Delta_p = \omega_p - \omega_{eg}$, $\Delta_c = \omega_c - \omega_{re}$, $\Delta_1 = \omega_1 - \omega_{eb}$, $\Delta_2 = \Delta_p + \Delta_c$ is the two-photon detuning and $\sigma_{\alpha\beta}^j = |\alpha\rangle_{jj}\langle\beta|$ is the transition operator for atom j at position $\mathbf{r}_j$. Using the Hamiltonian equation (1) we can write down the Heisenberg Langevin equations as

$$\begin{aligned} \dot{\sigma}_{eg}^j &= (i\Delta_p - \gamma_{eg})\sigma_{eg}^j - i\Omega_p(\sigma_{ee}^j - \sigma_{gg}^j) + i\Omega_c^*\sigma_{rg}^j \\ &\quad + i\Omega_1\sigma_{bg}^j, \\ \dot{\sigma}_{rg}^j &= [i(\Delta_2 - S(\mathbf{r})) - \gamma_{rg}]\sigma_{rg}^j + i\Omega_c\sigma_{eg}^j - i\Omega_p\sigma_{re}^j, \\ \dot{\sigma}_{bg} &= [i(\Delta_p - \Delta_1) - \Gamma]\sigma_{bg}^j + i\Omega_1^*\sigma_{eg}^j - i\Omega_p\sigma_{be}^j, \end{aligned} \tag{3}$$

where Γ is the relaxation rate of dipole-forbidden transition between $|g\rangle$ and $|b\rangle$ whereas $S(\mathbf{r})$ is the total vdW induced shift of Rydberg state $|r\rangle$ for an atom at position $\mathbf{r}$ and can therefore be written as

$$S(\mathbf{r}) = \sum_{i<j}^{n_{SA}} \Delta(\mathbf{r} - \mathbf{r}_j)\sigma_{rr}. \tag{4}$$

In eq. (4), σ_{rr} is the population of Rydberg state $|r\rangle$ and we can approximate it by a Lorentzian function. We consider the stationary-state solution of eq. (3) without considering vdW shift $S(\mathbf{r})$ and the average population of Rydberg state can then be calculated as [23,24]

$$\langle\sigma_{rr}\rangle = (\sigma_{rg})(\sigma_{gr}). \tag{5}$$

In the present consideration, the decay rate γ_{rg} and the dipole forbidden transition Γ are very weak, so we consider γ_{rg} and Γ equal to zero in our calculation. We also consider the resonance condition ($\Delta_1 = 0$) for control field Ω_1. From the steady-state solution of eq. (3) without considering the vdW interaction, we can write σ_{rg} as

$$\sigma_{rg} = \frac{[\Gamma + i(\Delta_1 - \Delta_p)]\Omega_c\Omega_p}{(\gamma_{rg} - i\Delta_2)|\Omega_1|^2 + [\Gamma + i(\Delta_1 - \Delta_p)]F}, \tag{6}$$

where $F = \gamma_{rg}(\gamma_{eg} - i\Delta_p) - \Delta_2(i\gamma_{eg} + \Delta_p) + |\Omega_c|^2$. Using the following approximations, *i.e.*, $\gamma_{rg} \ll \gamma_{eg}$ then the term $\gamma_{rg}(\gamma_{eg} - i\Delta_p) \to 0$ whereas $\Delta_p < \gamma_{eg}$ leads to $\Delta_p \to 0$ and $\gamma_{rg} \cong 0$, $\Gamma \cong 0$, $\Delta_1 \cong 0$, then the final form of σ_{rg} can therefore be written as

$$\sigma_{rg} = -\frac{\Omega_c\Omega_p}{|\Omega_c|^2 + \frac{\Delta_2}{\Delta_p}|\Omega_1|^2 - i\gamma_{eg}\Delta_2}. \tag{7}$$

The expression for population of Rydberg state may take the form

$$\langle\sigma_{rr}\rangle = \frac{|\Omega_c|^2|\Omega_p|^2}{(|\Omega_c|^2 + \frac{\Delta_2}{\Delta_p}|\Omega_1|^2)^2 + \gamma_{eg}^2\Delta_2^2}. \tag{8}$$

Further, we discuss about the vdW shift and consider that an atom is in a Rydberg state which induces a vdW shift $\Delta(R)$ for another atom located at a distance R. The vdW interaction suppresses the excitation of all the atoms in a small volume V_{SA}, which is called as a Rydberg blockade or superatom (SA) [22]. There is only one Rydberg

excited atom in each SA, *i.e.*, in V_{SA}. The number of atoms in a SA may be defined as $n_{SA} = \rho(\mathbf{r})V_{SA}$, where $\rho(\mathbf{r})$ is the atomic density. The total medium can then be treated as the collection of superatoms, and the number of superatoms in volume V will be $N_{SA} = \rho_{SA}V$. Then, the total vdW shift at position $\mathbf{r}$ can be written as [23,24]

$$S(\mathbf{r}) = \sum_{j}^{N_{SA}} \Delta(\mathbf{r}-\mathbf{r}_j)\Sigma_{RR}(\mathbf{r}_j) = \bar{\Delta}\Sigma_{RR}(\mathbf{r}) + s(\mathbf{r}), \quad (9)$$

where the first term in right side of eq. (9) shows the excited SA at $\mathbf{r}_j \approx \mathbf{r}$ *i.e.*, $\Sigma_{RR}(r) \to 1$, which induces divergent vdW shift in a volume of SA, and then $\Delta(0) \cong \frac{1}{V_{SA}}\int_{V_{SA}} \Delta r' \mathrm{d}^3 r' \to \infty$. The second part on the right side of eq. (9) shows the vdW shift induces the external SAs outside the volume and can be expressed as $s(\mathbf{r}) = \sum_j^{N_{SA}} \Delta(\mathbf{r}-\mathbf{r}_j)\Sigma_{RR}(\mathbf{r}_j)$. We can calculate the expression for $s(\mathbf{r})$ by replacing the summation by integration over the total volume and using the mean field approximation as [23]

$$\langle s(\mathbf{r})\rangle = \frac{w}{8}\langle \Sigma_{RR}(\mathbf{r})\rangle, \quad (10)$$

where w is the half-width of Lorentzian function of population in Rydberg state given by $|\Omega_c|^2/\gamma_{eg}$. To find the analytical expression for $s(\mathbf{r})$, we need to calculate $\Sigma_{RR}(\mathbf{r})$. The dynamics of individual SAs can be described in the form of collective states and operators within the blockade volume such that the ground and single collective Rydberg excited state are given by $|G\rangle = |g_1, g_2, g_3, \ldots, g_{n_{SA}}\rangle$ and $|R^{(1)}\rangle = \frac{1}{\sqrt{n_{SA}}} \times \sum_j^{n_{SA}} |g_1, g_2, g_3, \ldots, \mathbf{r}_j, \ldots, g_{n_{SA}}\rangle$ [23], where $g_1, g_2, \ldots, g_{n_{SA}}$ are the ground states of the atoms in SAs, whereas $|R^{(1)}\rangle$ shows that in a SA one atom must be in Rydberg state.

For a single-atom treatment and considering a SA in state $|G\rangle$, $\Sigma_{RR}(r)$ can be represented as [23]

$$\Sigma_{RR} = (\Sigma_{RG})(\Sigma_{GR}), \quad (11)$$

where

$$\Sigma_{RG} = \frac{\sqrt{n_{SA}}\Omega_c\Omega_p\Sigma_{GG}}{\Delta_2(i\gamma_{eg}+\Delta_p) - (\frac{\Delta_2}{\Delta_p}|\Omega_1|^2 + |\Omega_c|^2)}. \quad (12)$$

Using eqs. (11) and (12) with considering $\Sigma_{GG}+\Sigma_{RR} = 1$, the expression for Σ_{RR} after some mathematical steps can be calculated as

$$\Sigma_{RR} = \frac{n_{SA}|\Omega_c|^2|\Omega_p|^2}{|\Omega_c|^2|\Omega_p|^2 n_{SA} + B + \gamma_{eg}^2\Delta_2^2}, \quad (13)$$

where $B = [\Delta_2\Delta_p - (|\Omega_c|^2 + \frac{\Delta_2}{\Delta_p}|\Omega_1|^2)]^2$.

The compact expression for optical susceptibility of our proposed atomic system can therefore be written as

$$\chi = \xi\Bigg[\Sigma_{RR}\frac{\Delta_p}{(-i\Delta_p)(\gamma_{eg}-i\Delta_p)+|\Omega_1|^2} + (1-\Sigma_{RR}) \times \frac{\Delta_p}{(-i\Delta_p)(\gamma_{eg}-i\Delta_p)+A}\Bigg], \quad (14)$$

where $\xi = \frac{2N_{SA}|\mu_{eg}|^2}{\hbar\epsilon_0}$ and $A = |\Omega_1|^2 + |\Omega_c|^2[\gamma_{eg} - i(\Delta_2 - \langle s(r)\rangle)]^{-1}$. From eq. (13), it is clear that Σ_{RR} depends on n_{SA} which is directly related to the superatoms. The blockade effects arise from the dipole-dipole interactions between atoms. Thus, the blockade effect modifies the susceptibility of the system as shown in eq. (14). For the case, when the blockade effect is so strong, *i.e.*, $\Sigma_{RR} \to 1$ the probe field sees a three-level with energy levels $|g\rangle$, $|e\rangle$ and $|b\rangle$ electromagnetically induce transparency (EIT) system. On the contrary, for non-interacting atoms, $\Sigma_{RR} \to 0$ whole the system reduces to a single inverse-Y configuration.

Results and discussion. – We start our discussion by considering an optical susceptibility (χ) of the atomic medium consist of Rydberg atoms (^{87}Rb). It is well known from the literature that the susceptibility of a medium is related with the refractive index via the relation

$$n = \sqrt{1+\chi} \approx 1 + \chi/2, \quad (15)$$

where $\chi = \chi_R + i\chi_I$, with real (χ_R) and imaginary (χ_I) parts of the optical susceptibility. Whereas $n = n_0 + n_R + in_I$, with real (n_R) and imaginary (n_I) parts, and $n_0 = 1$ is the background refractive index of the medium. We follow the same approach as described earlier in ref. [19] and consider two different coupling fields side by side each having the same Gaussian intensity profile. The optical susceptibility of the probe field varies in the transverse direction of x. The intensity distribution of the coupling beams can then be represented as [19]

$$I_c(x) = A\left(e^{\frac{-(x-a)^2}{2\sigma^2}} + e^{\frac{-(x+a)^2}{2\sigma^2}}\right), \quad (16)$$

where A is constant, whereas $2a$ and σ are the separation between the two potential channels and beam waist, respectively. To introduce gain in one and loss in another waveguide, here, we consider two different coupling detunings ($\pm\Delta_c$). The refractive index of the medium, then varies only with the coupling intensity. The key point here is to find out the two coupling detunings for gain and loss simultaneously in a system. We study the variation of imaginary part of the optical susceptibility *vs.* coupling detuning (Δ_c) using eq. (14). The fixed parameters are $n_{SA} = 10$, $\gamma = 1\,\mathrm{MHz}$, $\Omega_1 = 2\gamma$, $\Omega_p = 0.05\gamma$, $\Delta_p = 0.01\gamma$, $\gamma_{eg} = \gamma$, and $\sigma = 3\lambda$ [19,23]. We plot the imaginary part of optical susceptibility *vs.* Δ_c for two different coupling field strengths as shown in fig. 2(a). The plot clearly shows that there is gain (loss) for $-\Delta_c(+\Delta_c)$ simultaneously in our system. For a more clear picture next we plot the Im[χ] *vs.* coupling field strength (Ω_c) by considering two coupling field detunings, *i.e.*, $\Delta_c = \pm 0.01\gamma$, see fig. 2(b). We indeed notice that for two different coupling field detunings ($\Delta_c = \pm 0.01\gamma$), the imaginary parts for gain and loss waveguides *vs.* coupling field strength are different. In comparison, the two curves in fig. 2(b) are flipped with each other with negative sign. We also study the real

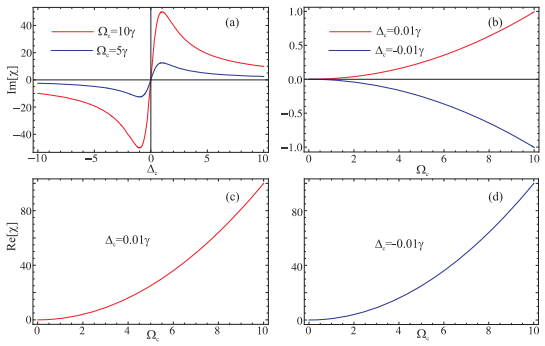

Fig. 2: (Color online) (a) The imaginary part of optical susceptibility (χ) *vs.* coupling field detuning (Δ_c) for $\Omega_c = 5\gamma$ and $\Omega_c = 10\gamma$. (b) The imaginary part of optical susceptibility (χ) *vs.* coupling field (Ω_c) for $\Delta_c = 0.01\gamma$ and $\Delta_c = -0.01\gamma$. (c) The real part of optical susceptibility (χ) *vs.* coupling field (Ω_c) when $\Delta_c = 0.01\gamma$. (d) The real part of optical susceptibility (χ) *vs.* coupling field (Ω_c) when $\Delta_c = -0.01\gamma$, the other parameters are presented in the text.

part of optical susceptibility and plot it *vs.* coupling field strength for two coupling field detunings ($\pm 0.01\gamma$). It is found that the real part of optical susceptibility associated with two waveguides overlap with each other. Figures 2(c) and (d) represent the Re[χ] for loss and gain waveguides, respectively.

Now, it is established from the relation between the optical susceptibility and the coupling field strength Ω_c as depicted in fig. 2(b) that we can achieve a spatial index modulation. We use the intensity distribution as described in eq. (16) and relate this with eq. (15), then the refractive index becomes a position dependent, *i.e.*, $n(x)$. To study the refractive index of the medium, we consider two different coupling field detunings ($\pm\Delta_c$) for gain and loss waveguides and plot the real and imaginary parts of the refractive index *vs.* x. First, we consider $\Delta_c = -0.01\gamma$ (gain) and 0.01γ (loss) for two coupling field detunings and choose all the other parameters as described in the text. We plot the real and imaginary parts of the refractive index *vs.* position x as depicted in figs. 3(a), (b). The plots clearly reveal that the real part of the refractive index is an even function of x, while the imaginary part is an odd function of x. The imaginary part of $n(x)$ describes that the gain and loss remain the same and balance each other. The $\mathcal{PT}$-symmetry demands that the real (imaginary) part must be even (odd) function of position x and the gain (loss) must be balanced to each other. Following the above statement our investigation fulfills the requirements of $\mathcal{PT}$-symmetry. Further, we proceed our investigation and confirm that the realization of $\mathcal{PT}$-symmetry is valid for all those values where ($-\Delta_c = +\Delta_c$). For different values of coupling field detunings where $-\Delta_c = +\Delta_c$, we plot the real and imaginary parts of the refractive index *vs.* x. We get an even (odd) function for the real (imaginary) part of refractive index with balance loss (gain), see figs. 3(a)–(h).

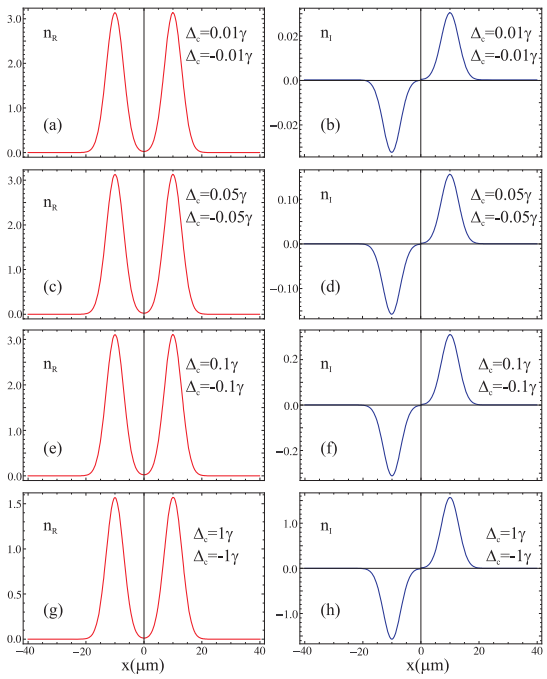

Fig. 3: (Color online) The real and imaginary parts of refractive indexes as a function of position x for ((a), (b)) $\Delta_c = 0.01\gamma$ and $\Delta_c = -0.01\gamma$, ((c), (d)) $\Delta_c = 0.05\gamma$ and $\Delta_c = -0.05\gamma$, ((e), (f)) $\Delta_c = 0.1\gamma$ and $\Delta_c = -0.1\gamma$, and ((g), (h)) $\Delta_c = 1\gamma$ and $\Delta_c = -1\gamma$, the other parameters are the same as in the text.

To study the perfect situation of $\mathcal{PT}$-symmetric systems, *i.e.*, to achieve the perfect symmetric real and antisymmetric imaginary parts of the refractive index of the medium. Here, we define an error function as

$$\psi(x) \cong n(x) - n^*(-x) \approx 0, \tag{17}$$

where $n(x) \approx 1 + \frac{1}{2}\chi(x)$. For the realization of $\mathcal{PT}$-symmetry, it is important to make the error function $\psi(x)$ equal or close to zero. Earlier, in an atomic system of two species the real and imaginary parts of the error function have been noticed and found it 1% and 2% of the real and imaginary parts of $n(x)$, respectively [17]. Similarly, in a single species of atomic medium the real and imaginary parts of the error function is calculated as below 5%. We explore the error function and found that the real and imaginary parts of the error function $\psi(x)$ are 0.0006% and 0.03% of the real and imaginary parts of $n(x)$. We believe that in our proposed scheme the error function approaches to zero.

The control of $\mathcal{PT}$-symmetry is an important characteristic via external parameters. In the present scheme we can control the $\mathcal{PT}$-symmetry using different parameters, these include for example, coupling field detuning, strength of probe and control fields. As mentioned earlier that $\mathcal{PT}$-symmetry is satisfied for $-\Delta_c = +\Delta_c$.

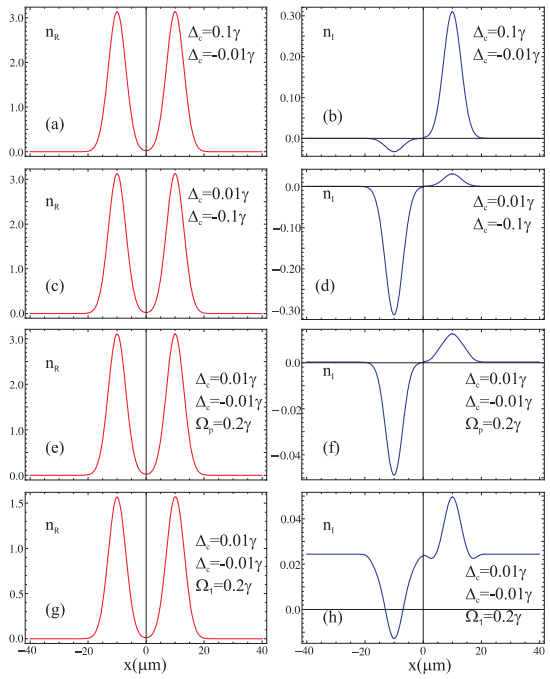

Fig. 4: (Color online) The real and imaginary parts of refractive indexes as a function of position x for ((a), (b)) $\Delta_c = 0.1\gamma$ and $\Delta_c = -0.01\gamma$, ((c), (d)) $\Delta_c = 0.01\gamma$ and $\Delta_c = -0.1\gamma$, ((e), (f)) $\Delta_c = 0.01\gamma$, $\Delta_c = -0.01\gamma$, and $\Omega_p = 0.2\gamma$ and ((g), (h)) $\Delta_c = 0.01\gamma$, $\Delta_c = -0.01\gamma$ and $\Omega_1 = 0.2\gamma$, the other parameters are the same as in the text.

Now we consider two coupling field detunings with different strengths, *i.e.*, $\Delta_c = 0.1\gamma$ and -0.01γ, while keeping all the other parameters remain the same as used in fig. 3. We again plot the real and imaginary parts of refractive index *vs.* position function x, see figs. 4(a), (b). The $\mathcal{PT}$-symmetry breaks due to imbalance gain and loss in the system simultaneously as shown in fig. 4(b). It is due to the fact that $\Delta_c = 0.1\gamma$ in loss waveguide is greater than in gain waveguide ($\Delta_c = -0.01\gamma$). It is also clear from the realization of $\mathcal{PT}$-symmetry that the gain and loss must balance each other simultaneously in a system. Therefore, symmetry breaking occurs in our system by considering different strengths of coupling field detunings and then the medium treated as non-$\mathcal{PT}$-symmetric. Similarly, we consider $\Delta_c = 0.01\gamma$ and -0.1γ for loss and gain waveguides and plot the real and imaginary parts of the refractive index *vs.* position x, see figs. 4(c), (d). In this time $\Delta_c = -0.1\gamma$ in gain waveguide is greater than in loss waveguide ($\Delta_c = 0.01\gamma$) and we get a symmetry breaking again with a large gain in the system as shown in fig. 4(d). This clearly indicates that symmetry breaking occurs in our system for different coupling field detunings, *i.e.*, $-\Delta_c \neq +\Delta_c$.

As our system is nonlinear and depends on the strength of probe field intensity. By changing the strength of probe field intensity one can modify the characteristics of a medium. From an earlier investigation where a strong interacting three-level Rydberg atomic medium has been considered and modified the EIT features by changing the probe field intensity [23]. Our system is an extension of the previous work [23] and also dependent on the intensity of probe field. Here, we expect that the probe field intensity will modify the characteristics of $\mathcal{PT}$-symmetric medium. We choose $\Delta_c = \pm 0.01\gamma$ and increase the strength of probe field intensity from 0.05γ to 0.2γ and plot the real and imaginary parts *vs.* position x, see figs. 4(e), (f). It is found that by increasing the strength of probe field intensity, the gain and loss in a system become unbalanced. Symmetry breaking occurs via increasing the strength of probe field and the medium becomes non-$\mathcal{PT}$-symmetric. Further, $\mathcal{PT}$-symmetry also depends on the control field intensity (Ω_1) in our system and symmetry breaking occurs for $\Omega_1 < 1.3\gamma$. We choose $\Delta_c = \pm 0.01\gamma$, $\Omega_p = 0.05\gamma$, $\Omega_1 = 0.2\gamma$, and plot the real and imaginary parts of refractive index *vs.* position x, see in figs. 4(g), (h). The plot in fig. 4(h) shows that the medium becomes an absorptive with unequal gain and loss.

To study a more clear picture about $\mathcal{PT}$-symmetry, next we consider the wave propagation along the z-direction through the proposed atomic medium as shown in fig. 1(a). We try to show that the propagation constant has real value under the condition of $\mathcal{PT}$-symmetry. Using the paraxial approximation one can write the field equation [17] as

$$i\frac{\partial \mathcal{E}_p}{\partial z} + \frac{1}{2k_p}\frac{\partial^2 \mathcal{E}_p}{\partial x^2} + \frac{1}{2}k_p\chi_p(x)\mathcal{E}_p = 0, \tag{18}$$

where k_p describe the wave vector of probe field and

$$\mathcal{E}_p(z,x) = E(x)e^{ibz}, \tag{19}$$

with b being the propagation constant and can show that the field would be attenuated quickly during propagation in the medium when b has non-zero imaginary part. In contrast, the field can propagate for longer distances through the medium if the imaginary part of b is very small or zero. To study the wave propagation through the medium, we are looking for eigenvalue problem instead of solving the field equation. We substitute eq. (19) into eq. (18) and make a simplified eigenvalue equation as

$$\frac{\mathrm{d}^2 E}{\mathrm{d}\xi^2} + \frac{k_p}{k_s^2}\chi(\xi)E = \beta E, \tag{20}$$

where $\beta = \frac{2k_p}{k_s^2}b$. To show the spectrum of β we plot Im[β] *vs.* different number of eigen modes for different conditions and link these results with the realization of $\mathcal{PT}$- and non-$\mathcal{PT}$-symmetry as investigated in figs. 3 and 4. As discussed above that for the realization of $\mathcal{PT}$-symmetric medium, the real (imaginary) part must be even (odd) and the gain and loss waveguide must balance each other

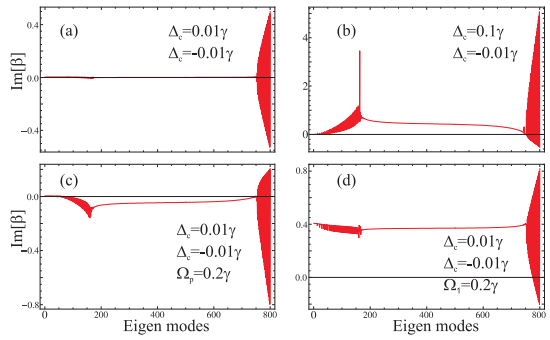

Fig. 5: (Color online) The spectrum of eigenvalue of Im[β] *vs.* different eigenmodes (a) $\mathcal{PT}$-symmetry and (b)–(d) non-$\mathcal{PT}$-symmetry.

simultaneously in a system, see fig. 3. For the realization of $\mathcal{PT}$-symmetric medium we expect that the Im[β] must be zero or close to zero. We choose the same parameters as used in figs. 3(a), (b), and plot the Im[β] *vs.* different eigen modes. The plot in fig. 5(a) portrays that the Im[β] is zero which satisfy the $\mathcal{PT}$-symmetry condition of figs. 3(a), (b). Next, we choose the unbalance gain and loss simultaneously in a system to satisfy the results obtained in figs. 4(a), (b). We consider all the parameters as used in figs. 4(a), (b), and plot the Im[β] *vs.* different modes. It is found that Im[β] has non-zero values for different modes and gives us a non-$\mathcal{PT}$-symmetric medium, see fig. 5(b). As described above that $\mathcal{PT}$-symmetry breaking occurs when the intensity of the probe (Ω_p) and control (Ω_1) fields varies, see figs. 4(e)–(h). To study the influence of these intensities over Im[β], we plot again Im[β] *vs.* different modes as shown in figs. 5(c) and (d). The results describe that Im[β] has non-zero values for different modes and the medium becomes a non-$\mathcal{PT}$-symmetric when the probe and control fields are varied.

Conclusion. – To conclude, we propose to use Rydberg atomic media consist of ^{87}Rb atoms in the four-level inverted Y-type configuration, to realize $\mathcal{PT}$-symmetric profiles of the refractive index. By varying the external parameters such as coupling field detuning (Δ_c), probe field intensity (Ω_p) and control field intensity (Ω_1), we investigate various index profiles, in particular the control over $\mathcal{PT}$- and non-$\mathcal{PT}$-symmetry via changing the external parameters. More interestingly, an exact $\mathcal{PT}$-symmetry can be achieved with different parameters in Rydberg atoms.

REFERENCES

[1] Bender C. M. and Boettcher S., *Phys. Rev. Lett.*, **80** (1998) 5243.
[2] Lee Y.-C., Hsieh M.-H., Flammia S. T. and Lee R.-K., *Phys. Rev. Lett.*, **112** (2014) 130404.
[3] Ruschhaupt A., Delgado F. and Muga J. D., *J. Phys. A*, **38** (2005) L171.
[4] Bender C. M., Brody D. C. and Jones H. F., *Phys. Rev. D*, **70** (2004) 025001.
[5] Goldsheid I. Y. and Khoruzhenko B. A., *Phys. Rev. Lett.*, **80** (1998) 2897.
[6] Rotter I., *J. Phys. A: Math. Theor.*, **42** (2009) 153001.
[7] Kulishov M., Laniel J. M., Be langer N., Azana J. and Plant D. V., *Opt. Express*, **13** (2005) 3068.
[8] Lin Z., Ramezani H., Eichelkraut T., Kottos T., Cao H. and Christodoulides D. N., *Phys. Rev. Lett.*, **106** (2011) 213901.
[9] Feng L., Xu Y.-L., Fegadolli W. S., Lu M.-H., Oliveira J. E. B., Almeida V. R., Chen Y.-F. and Scherer A., *Nat. Mater.*, **12** (2013) 108.
[10] Longhi S., *Phys. Rev. A*, **82** (2010) 031801.
[11] Chong Y. D., Ge L., Cao H. and Stone A. D., *Phys. Rev. Lett.*, **105** (2010) 053901.
[12] Konotop V. V., Shchesnovich V. S. and Zezyulin D. A., *Phys. Lett. A*, **376** (2012) 2750.
[13] Ziauddin, Chuang Y.-L. and Lee R.-K., *Phys. Rev. A*, **92** (2015) 013815.
[14] Benisty H., Degiron A., Lupu A., DeLustrac A., Chenais S., Forget S., Besbes M., Barbillon G., Bruyant A., Blaize S. and Lerondel G., *Opt. Express*, **19** (2011) 18004.
[15] Regensburger A., Bersch C., Miri M.-A., Onishchukov G., Christodoulides D. N. and Peschel U., *Nature (London)*, **488** (2012) 167.
[16] Schindler J., Li A., Zheng M. C., Ellis F. M. and Kottos T., *Phys. Rev. A*, **84** (2011) 040101(R).
[17] Hang C., Huang G. and Konotop V. V., *Phys. Rev. Lett.*, **110** (2013) 083604.
[18] Li H.-J., Dou J.-P. and Huang G., *Opt. Express*, **21** (2013) 32053.
[19] Sheng J., Miri M. A., Christodoulides D. N. and Xiao M., *Phys. Rev. A*, **88** (2013) 041803(R).
[20] Konotop V. V., Yang J. and Zezyulin D. A., arXiv:1603.06826 [nlin.PS].
[21] Gallagher T., *Rydberg Atoms* (Cambridge University Press) 2005.
[22] Lukin M. D., Fleischhauer M. and Cote R., *Phys. Rev. Lett.*, **87** (2001) 037901.
[23] Petrosyan D., Otterbach J. and Fleischhauer M., *Phys. Rev. Lett.*, **107** (2011) 213601.
[24] Petrosyan D., Höning M. and Fleischhauer M., *Phys. Rev. A*, **87** (2013) 053414.